THE JOURNAL OF PHYSICAL CHEMISTRY A
A JOURNAL OF THE AMERICAN CHEMICAL SOCIETY

pubs.acs.org/JPCA

Article

The Dog That Didn't Bark: A New Interpretation of Hypsoporphyrin Spectra and the Question of Hypsocorroles

Abhik Ghosh* and Jeanet Conradie*

Cite This: *J. Phys. Chem. A* 2021, 125, 9962–9968

Read Online

ACCESS | Metrics & More | Article Recommendations | Supporting Information

ABSTRACT: Nearly a half-century after Gouterman classified the UV–vis–NIR spectra of porphyrin derivatives as normal, hyper, or hypso, we propose a heretofore unsuspected "mechanism" underlying hypso spectra. Hypsoporphyrins, which exhibit blueshifted optical spectra relative to normal porphyrins (such as Zn porphyrins), typically involve d^n transition metal ions, where $n > 6$. The spectral blueshifts have been traditionally ascribed to elevated porphyrin e_g LUMO (lowest unoccupied molecular orbital) energy levels as a result of antibonding interactions with metal d_π orbitals. Herein, we have found instead that the blueshifts reflect a lowering of the a_{2u} HOMO (highest occupied molecular orbital) energy levels. Electronegative metals such as Pd and Pt transfer smaller quantities of electron density to the porphyrin nitrogens, compared to a more electropositive metal such as Zn. With large amplitudes at the porphyrin nitrogens, the a_{2u} HOMOs of Pd(II) and Pt(II) porphyrins accordingly exhibit lower orbital energies than those of Zn(II) porphyrins, thus explaining the hypso effect. Hypso spectra are also observed for corroles: compared with six-coordinate Al(III) corroles, which may be thought of exhibiting normal spectra, Au(III) corroles, for instance, exhibit blueshifted or hypso spectra.

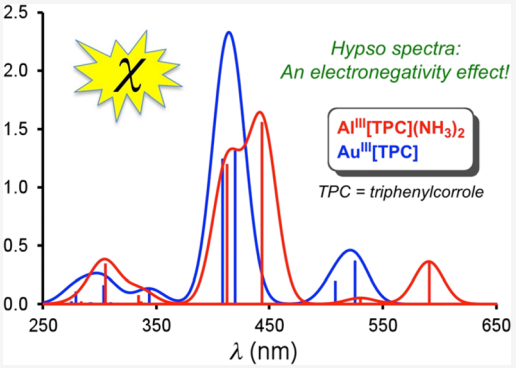

1. INTRODUCTION

The famous four-orbital model,[1,2] which explained the electronic absorption spectra of simple porphyrins, was devised by Gouterman in the early 1960s, while he was an Assistant Professor at Harvard. According to this model, the two highest occupied molecular orbitals (HOMOs) (a_{1u} and a_{2u} under D_{4h} symmetry) and the two lowest unoccupied molecular orbitals (LUMOs) (e_g) are energetically well-separated from all other occupied and virtual molecular orbitals (MOs). The Q and Soret bands are then explained by transitions between these four MOs, taking configuration interaction into account. Some 15 years later, now on West Coast, he presented an optical taxonomy of porphyrins in a lengthy chapter in Dolphin's multivolume work *The Porphyrins*.[3] He classified porphyrins into three major classes—normal, hypso, and hyper. Normal porphyrins exhibit electronic absorption spectra that can be largely accounted for with the four-orbital model. Hypsoporphyrins exhibit blueshifted spectra, typical examples including d^n metalloporphyrins for $n > 6$. In contrast, hyperporphyrins exhibit redshifted optical spectra and/or extra absorption bands above 300 nm. Typical examples include d^n metalloporphyrins with $n < 6$, which in turn include many heme proteins and their intermediates and model compounds. Substituents and other structural perturbations can also lead to hyper spectra.[4]

Many, but not all, hypsoporphyrins, especially the noble metal porphyrins, are moderately to strongly phosphorescent.[5−7] Their long-lived triplet states have been exploited for oxygen

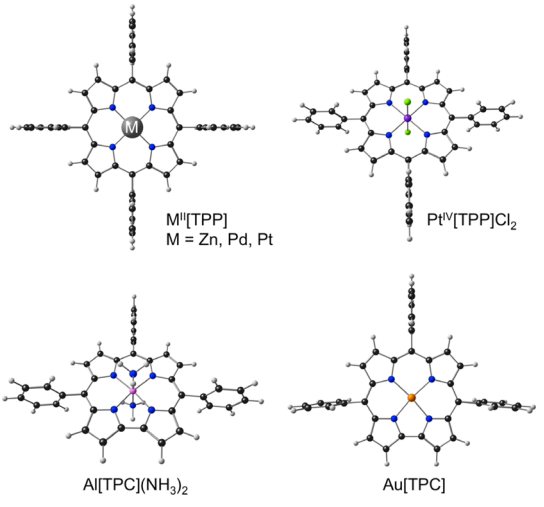

Figure 1. Molecules studied in this work.

Received: September 24, 2021
Revised: October 21, 2021
Published: November 11, 2021

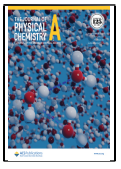

https://doi.org/10.1021/acs.jpca.1c08425
J. Phys. Chem. A 2021, 125, 9962–9968

Table 1. Comparison of TDDFT and Experimental Absorption Maxima (nm)[a]

	Q (nm)					Soret (nm)					HOMO−LUMO gap (eV)			
compound	OLYP	B3LYP	B3LYP*	CAMY-B3LYP	Expt	OLYP	B3LYP	B3LYP*	CAMY-B3LYP	Expt	OLYP	B3LYP	B3LYP*	CAMY-B3LYP
Zn[TPP]	564.3	531.2	542.0	540.4	589	454.3	432.6	441.8	424.8	425	1.94	2.90	2.63	4.42
Pd[TPP]	534.9	507.0	515.6	512.7	554	445.6	422.1	430.7	412.2	418	2.09	3.04	2.78	4.58
Pt[TPP]	519.7	493.7	500.2	494.5	539	437.5	413.2	420.7	400.3	493	2.19	3.14	2.89	4.68
Pt[*TPP*]Cl_2	673.1	600.3	583.2	523.3	570	445.7	423.8	431.4	414.8	421	1.81	2.87	2.72	4.50
	544.0	516.3	524.5	516.5										
Au[TPC]	554.4	525.9	534.6	530.3	575	449.4	419.4	429.8	408.1	418	1.85	2.75	2.51	4.26
	537.8	508.3	516.7	507.4	560	441.2	408.4	418.5	391.8					
Al[TPC]-$(NH_3)_2$	631.7	590.7	607.6	600.7	620	471.8	443.4	455.9	436.4	432	1.55	2.46	2.20	3.94
	570.9	530.4	544.2	528.1	582	445.4	413.0	424.3	398.0	412				

[a]The experimental data quoted are obtained from refs 40−44.

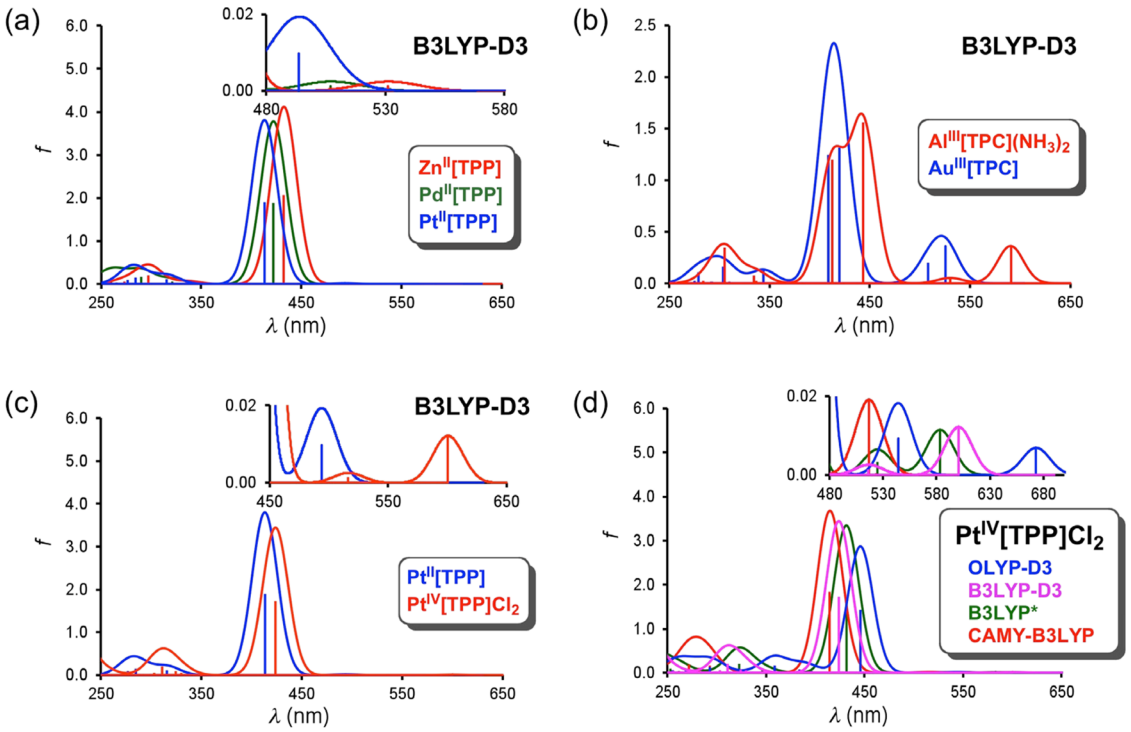

Figure 2. TDDFT (COSMO/dichloromethane) simulated spectra of the metalloporphyrins studied.

sensing and photodynamic therapy.[8−12] Gouterman and coworkers famously exploited platinum(II) porphyrins to devise pressure-sensitive paints for airplane wings.[13−16] More recently, 5d metallocorroles,[17−21] including ReO,[22−24] OsN,[25,26] Ir,[27−29] Pt,[30,31] and Au[20,32−35] corroles, have been found to exhibit NIR phosphorescence under ambient conditions, raising the question whether they, or at least some of them, should be described as hypsocorroles.

Remarkably, in spite of their broad importance, few hypso and hyper spectra have been examined by means of modern quantum chemical methods, such as time-dependent density functional theory (TDDFT) calculations,[36−38] which prompted us to undertake a first such investigation of selected hypsoporphyrin systems. Thus, we examined several M^{II}[TPP] derivatives (where M = Zn,[39,40] Pd,[41] and Pt[41]), Pt^{IV}[TPP]-Cl_2,[42] and two corroles, Al^{III}[TPC]$(NH_3)_2$[43] and Au^{III}[TPC][34] (Figure 1). Of these, only Pd^{II}[TPP] and Pt^{II}[TPP] are clearly hypsoporphyrins, while Au[TPC] is a potential hypsocorrole. The other complexes are included for comparison.

The hypso effect has traditionally been explained in terms of metal(d_π)−porphyrin(LUMO) orbital interactions.[3] By engaging in backbonding interactions with the porphyrin e_g LUMOs, the d_{xz} and d_{yz} orbitals are stabilized. The corresponding antibonding MOs, that is, the LUMOs, the theory goes, are destabilized, which results in an elevated HOMO−LUMO gap, explaining the hypsochromic shifts of the Q and Soret bands. To our surprise, the present reinvestigation provided no support whatsoever for this long-held picture, suggesting instead an entirely different "mechanism" underlying hypso spectra.

2. COMPUTATIONAL METHODS

All calculations were carried out with the ADF[44] 2018 program with all-electron ZORA-STO-TZ2P basis sets, fine meshes for numerical integration of matrix elements, and adequately tight convergence criteria for both SCF and geometry optimization cycles. Molecular geometries were optimized with OLYP[45,46]-D3,[47] with D_{4h} and C_{2v} symmetry constraints for the porphyrin and corrole derivatives, respectively. These optimized geo-

https://doi.org/10.1021/acs.jpca.1c08425
J. Phys. Chem. A 2021, 125, 9962−9968

Table 2. B3LYP-D3/STO-TZ2P TDDFT Results, Including Transition Energies (E) and Wavelengths (l), Oscillator Strengths (f), MO Compositions, and Symmetries

molecule	peak	E (eV)	λ (nm)	f	MO composition		weight (%)	state symmetry
					from	to		
Zn[TPP]	Q	2.33	531.2	0.001	HOMO	LUMO	55	E_u
					HOMO − 1	LUMO	45	E_u
	Soret	2.87	432.6	2.061	HOMO − 1	LUMO	54	E_u
Pd[TPP]	Q	2.45	507.0	0.001	HOMO − 1	LUMO	50	E_u
					HOMO	LUMO	49	E_u
	Soret	2.94	422.1	1.891	HOMO	LUMO	49	E_u
					HOMO − 1	LUMO	49	E_u
Pt[TPP]	Q	2.51	493.7	0.010	HOMO − 1	LUMO	55	E_u
					HOMO	LUMO	44	E_u
	Soret	3.00	413.2	1.906	HOMO	LUMO	54	E_u
					HOMO − 1	LUMO	44	E_u
Pt[TPP]Cl_2	Q	2.07	600.3	0.012	HOMO	LUMO	100	A_{2u}
		2.40	516.3	0.001	HOMO	LUMO + 1	55	E_u
					HOMO − 1	LUMO + 1	44	E_u
	Soret	2.93	423.8	1.722	HOMO − 1	LUMO + 1	54	E_u
					HOMO	LUMO + 1	42	E_u
Au[TPC]	Q	2.36	525.9	0.362	HOMO	LUMO	88	B_2
					HOMO − 1	LUMO + 1	11	B_2
		2.44	508.3	0.204	HOMO − 1	LUMO	81	A_1
					HOMO	LUMO + 1	18	A_1
	Soret	2.96	419.4	1.312	HOMO	LUMO + 1	80	A_1
					HOMO − 1	LUMO	17	A_1
		3.04	408.4	1.248	HOMO − 1	LUMO + 1	87	B_2
					HOMO	LUMO	11	B_2
Al[TPC]$(NH_3)_2$	Q	2.10	590.7	0.362	HOMO	LUMO	91	B_2
					HOMO − 1	LUMO + 1	8	B_2
		2.34	530.4	0.052	HOMO − 1	LUMO	60	A_1
					HOMO	LUMO + 1	39	A_1
	Soret	2.80	443.4	1.561	HOMO	LUMO + 1	59	A_1
					HOMO − 1	LUMO	39	A_1
		3.00	413.0	1.204	HOMO − 1	LUMO + 1	91	B_2
					HOMO	LUMO	7	B_2

metries were then used for TDDFT calculations with the OLYP-D3, B3LYP* (15% exact exchange), and CAMY-B3LYP[48−50] functionals. B3LYP[51,52]-D3-optimized geometries were used for the TDDFT calculations with the B3LYP functional. The COSMO[53] solvation model (with dichloromethane as the solvent) was used throughout.

3. RESULTS AND DISCUSSION

3.1. Theoretical Model. We began by examining to what extent TDDFT calculations reproduce known trends in relative positions of the absorption maxima of the compounds studied. As mentioned above, four exchange-correlation functionals were examined—OLYP-D3, B3LYP-D3, B3LYP*, and CAMY-B3LYP—with solvation (dichloromethane) taken into account with the COSMO model. Table 1 lists calculated and experimental absorption maxima and calculated HOMO−LUMO gaps, while Figure 2 presents selected simulated spectra, mostly from B3LYP-D3 calculations. It is immediately obvious that all the exchange-correlation functionals do a qualitatively good job of reproducing key trends in experimental absorption maxima. Thus, both the Q and Soret bands of Pd^{II}[TPP] and Pt^{II}[TPP] are hypsochromically shifted relative to those of Zn^{II}[TPP], with larger blueshifts for Pt, just as experimentally observed.[39−41] The calculations also predict a substantial spectral blueshift for Au^{III}[TPC] relative to Al[TPC]$(NH_3)_2$, mirroring a qualitatively similar blueshift for Au^{III}[TPFPC] relative to Al^{III}[TPFPC](py)$_2$.[33,43] Finally, the calculations predict a spectral redshift for Pt^{IV}[TPP]Cl_2 relative to Pt^{II}[TPP], again in qualitative accord with experimental results.[41,42]

Interestingly, the lowest-energy Q band of Pt^{IV}[TPP]Cl_2 appears to pose a peculiar challenge for some of the functionals. Thus, the calculated lowest-energy transition for this compound (experimental value:570 nm[42]) is not a true Q band but a HOMO(a_{2u}) → LUMO(a_{1g}) transition, where the a_{1g} LUMO corresponds to the empty d_{z2} orbital of the Pt(IV) center. Table 1 shows that while OLYP unduly redshifts this feature, CAMY-B3LYP results in an undue blueshift, whereas B3LYP-D3 and B3LYP* perform just about right.

3.2. MO Analysis. A first step toward understanding the hypsoporphyrin effect is to examine the MO composition of the various calculated spectral features. This information is provided in Table 2 for the B3LYP-D3 functional, while key MOs are depicted in Figure 3 for one of the complexes, Pt^{II}[TPP]. To our considerable surprise, we found that the four frontier MOs of all the complexes examined, except Pt^{IV}[TPP]Cl_2, correspond to classic Gouterman MOs, with little or no metal d character. Even for the two corrole derivatives, the four frontier MOs for Au^{III}[TPC] (Figure 4) and Al^{III}[TPC]$(NH_3)_2$ look essentially identical. This finding, reminiscent of the Sherlock Holmes story (*Silver Blaze*) about "the dog that didn't bark in the night-time",

https://doi.org/10.1021/acs.jpca.1c08425
J. Phys. Chem. A 2021, 125, 9962−9968

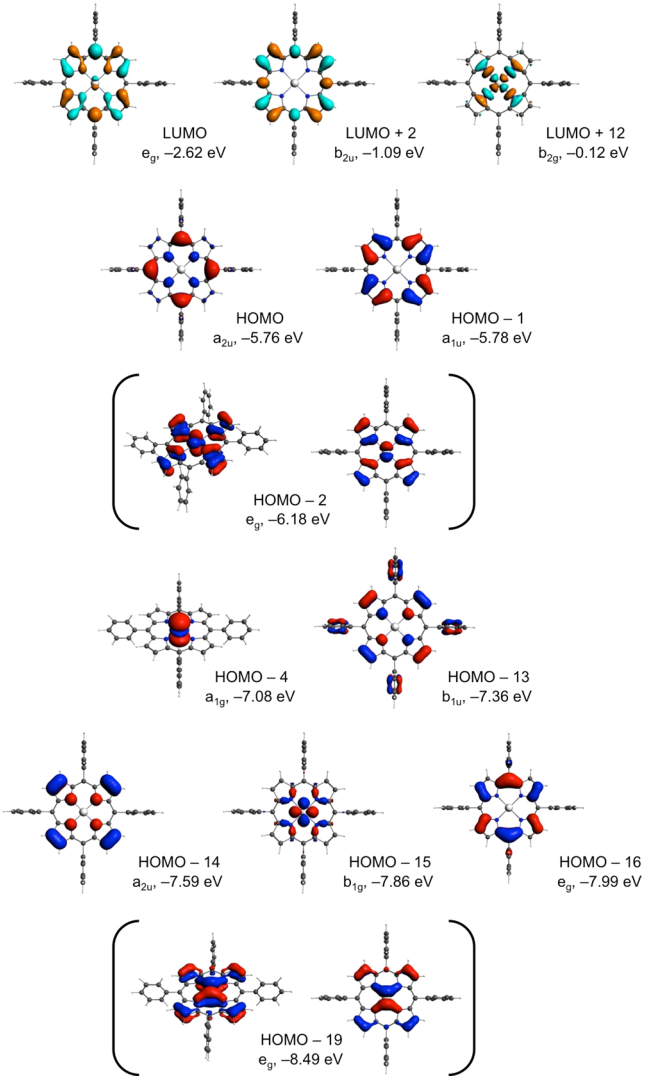

Figure 3. Selected B3LYP-D3 frontier MOs of Pt^{II}[TPP].

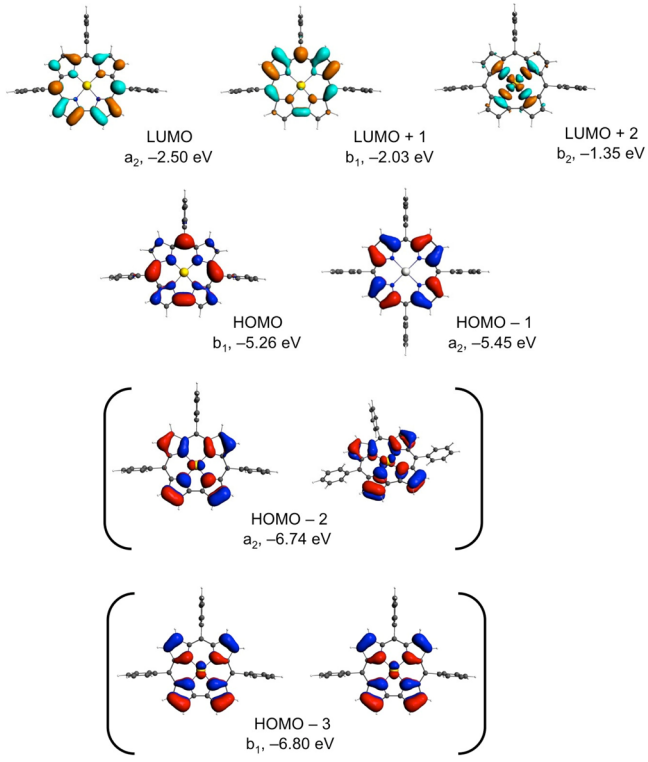

Figure 4. Selected B3LYP-D3 frontier MOs of Au^{III}[TPC].

flies in the face of—and indeed invalidates—the conventional explanation for the hypsoporphyrin effect, namely, that a π-antibonding interaction with the metal d_π orbitals is responsible for an elevation of the orbital energies of the e_g LUMOs.

A comparative study of the frontier MO energy levels (Figures 5 and 6) came to our rescue. While the LUMO energy levels were found to be almost identical across all the porphyrin (or corrole) derivatives studied, the hypsoporphyrins examined exhibit lower orbital energies for the a_{2u} HOMOs (or for the topologically similar b_1 HOMOs of corroles). This, then, appears to be the new explanation for the hypsoporphyrin effect.

3.3. Molecular Charge Distributions. The question as to why hypsoporphyrins such as Pd^{II}[TPP] and Pt^{II}[TPP], as well as hypsocorroles such as Au^{III}[TPC], should exhibit lower "a_{2u}" energy levels is a somewhat subtle one, because, as mentioned, there is little difference in the shape of these orbitals relative to those of the normal porphyrin Zn^{II}[TPP] [and the normal corrole Al^{III}[TPC]$(NH_3)_2$]. An examination of the atomic Mulliken and Hirschfeld charges, as well as of the nitrogen 1s orbital energies (Table 3), suggests a plausible explanation. Hypsoporphyrins appear to involve less electropositive metals that transfer less electron density to the porphyrin/corrole ligands as a whole and specifically to the macrocycle nitrogens. Thus, both the macrocyclic ligands as a whole and their central nitrogens carry less negative Hirschfeld charges in the case of the hypsoporphyrins, relative to the normal porphyrin Zn^{II}[TPP]. As a result, the nitrogen 1s orbital energies are also relatively more negative, which would translate to higher XPS ionization potentials, for the hypsoporphyrins. Given that the a_{2u} HOMO has large amplitudes on the macrocycle nitrogens, it follows that hypsoporphyrins should also exhibit lower a_{2u} orbital energies, which accounts for the hypsoporphyrin effect.

The above argument might suggest that a Pt(IV) porphyrin would exhibit a stronger hypsochromic shift than a Pt(II) porphyrin. As shown in Table 1, the opposite is observed. A recent, combined X-ray absorption spectroscopy and density functional theory (DFT) study has shown that a Pt(IV) porphyrin entails substantial oxidation of the porphyrin ligand as a whole.[54] That systemic oxidation results in a lowering of not only the a_{2u} HOMO, but also an even greater lowering of the e_gLUMOs, which explains the lack of a hypsoporphyrin spectrum for Pt^{IV}[TPP]Cl_2.

4. CONCLUSIONS

DFT and TDDFT calculations indicate that the hypsoporphyrin effect (blueshifted Q and Soret bands) does not result from elevated porphyrin LUMO (e_g) energy levels as a result of antibonding interactions with metal d_π orbitals. Instead the observed blueshifts reflect a lowering of the a_{2u} HOMO energy level. Electronegative metals such as Pd and Pt transfer smaller quantities of electron density to the porphyrin nitrogens, compared to a more electropositive metal such as Zn. As a result, the nitrogens in Pd and Pt porphyrins exhibit higher electrostatic potentials, more negative N 1s orbital energies, and higher N 1s ionization potentials. With large amplitudes at the porphyrin nitrogens, the a_{2u} HOMOs of Pd(II) and Pt(II) porphyrins also exhibit lower orbital energies (mirroring the behavior of the N 1s

https://doi.org/10.1021/acs.jpca.1c08425
J. Phys. Chem. A 2021, 125, 9962−9968

Table 3. Selected Mulliken and Hirschfeld Charges and N 1s Orbital Energies (eV) for the Compounds Studied

		Mulliken		Hirschfeld		N 1s energy	
		OLYP	B3LYP-D3	OLYP	B3LYP-D3	OLYP	B3LYP-D3
Zn^{II}[TPP]	M	0.815	0.817	0.479	0.481		
	ligand	−0.815	−0.817	−0.479	−0.481		
	N	−0.517	−0.519	−0.160	−0.170	−381.668	−390.126
	Cα	0.228	0.228	0.024	0.029		
	Cβ	0.236	0.190	−0.068	−0.067		
	C*m*	−0.020	−0.034	−0.005	−0.004		
Pd^{II}[TPP]	M	0.991	0.901	0.437	0.472		
	ligand	−0.991	−0.901	−0.437	−0.472		
	N	−0.550	−0.547	−0.158	−0.174	−382.396	−390.790
	Cα	0.221	0.227	0.019	0.024		
	Cβ	0.241	0.196	−0.066	−0.065		
	C*m*	−0.016	−0.032	−0.007	−0.006		
Pt^{II}[TPP]	M	0.975	0.933	0.249	0.263		
	ligand	−0.975	−0.933	−0.249	−0.263		
	N	−0.582	−0.571	−0.124	−0.138	−382.644	−391.036
	C_α	0.228	0.226	0.022	0.028		
	C_β	0.247	0.200	−0.065	−0.064		
	C_m	−0.014	−0.030	−0.005	−0.004		
Pt^{IV}[TPP]Cl_2	M	1.040	1.075	0.510	0.555		
	ligand	−0.355	−0.344	0.072	0.033		
	N	−0.515	−0.513	−0.113	−0.132	−383.100	−391.404
	Cα	0.250	0.244	0.030	0.035		
	Cβ	0.262	0.216	−0.054	−0.053		
	C*m*	−0.016	−0.029	0.000	0.000		
Au^{III}[TPC]	M	1.461	1.362	0.551	0.583		
	ligand	−1.461	−1.362	−0.551	−0.583		
	N2	−0.629	−0.607	−0.130	−0.142	−382.740	−391.090
	N1	−0.594	−0.573	−0.136	−0.150	−382.663	−391.089
	Cα	0.209	0.200	0.012	0.016		
	Cβ	0.219	0.182	−0.072	−0.072		
	C*m*	−0.056	−0.068	−0.017	−0.017		
Al^{III}[TPC]$(NH_3)_2$	M	1.660	1.640	0.390	0.424		
	ligand	−1.826	−1.817	−0.929	−0.938		
	N2	−0.635	−0.634	−0.155	−0.170	−381.014	−389.439
	N1	−0.548	−0.559	−0.159	−0.175	−381.191	−389.621
	N (NH_3)	0.237	0.163	−0.167	−0.186	−381.875	−390.341
	Cα	0.203	0.192	0.016	0.022		
	Cβ	0.196	0.157	−0.087	−0.086		
	C*m*	−0.074	−0.072	−0.022	−0.020		

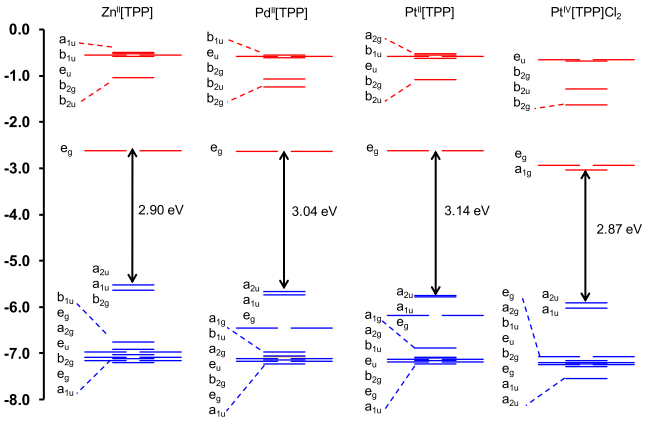

Figure 5. B3LYP-D3 MO energy level diagrams for key TPP derivatives studied.

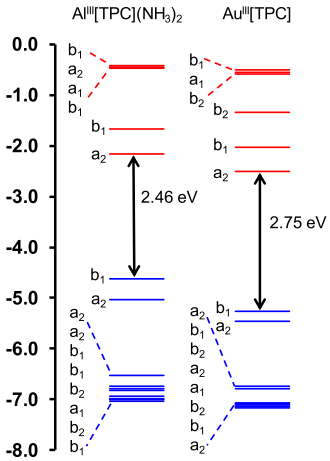

Figure 6. B3LYP-D3 MO energy level diagrams for key TPC derivatives.

https://doi.org/10.1021/acs.jpca.1c08425
J. Phys. Chem. A 2021, 125, 9962−9968

orbitals) than Zn(II) porphyrins, thus explaining the hypsoporphyrin spectra.

The hypsoporphyrin concept also appears to extend to corroles. With blueshifted spectral features relative to six-coordinate Al(III) corroles, Au(III) corroles appear to be justifiably described as hypsocorroles. It may be recalled that examples hypercorroles, likewise, have also been documented in the literature.[55]

■ ASSOCIATED CONTENT

Supporting Information

The Supporting Information is available free of charge at https://pubs.acs.org/doi/10.1021/acs.jpca.1c08425.

Optimized Cartesian coordinates (PDF)

■ AUTHOR INFORMATION

Corresponding Authors

Abhik Ghosh − *Department of Chemistry, UiT—The Arctic University of Norway, Tromsø N-9037, Norway;* orcid.org/0000-0003-1161-6364; Email: abhik.ghosh@uit.no

Jeanet Conradie − *Department of Chemistry, UiT—The Arctic University of Norway, Tromsø N-9037, Norway; Department of Chemistry, University of the Free State, Bloemfontein 9300, Republic of South Africa;* orcid.org/0000-0002-8120-6830; Email: conradj@ufs.ac.za

Complete contact information is available at: https://pubs.acs.org/10.1021/acs.jpca.1c08425

Notes

The authors declare no competing financial interest.

■ ACKNOWLEDGMENTS

This work was supported by grant no. 262229 and of the Research Council of Norway (AG) and grant nos. 129270 and 132504 of South African National Research Foundation.

■ REFERENCES

(1) Gouterman, M.; Wagniére, G. H.; Snyder, L. C. Spectra of Porphyrins. Part II. Four-Orbital Model. *J. Mol. Spectrosc.* **1963**, *11*, 108−127.

(2) For a recent biography of Martin Gouterman, see Ghosh, A. An Exemplary Gay Scientist and Mentor: Martin Gouterman (1931−2020). *Angew. Chem., Int. Ed.* **2021**, *60*, 9760−9770.

(3) Gouterman, M. Optical Spectra and Electronic Structure of Porphyrins and Related Rings. In *The Porphyrins*; Dolphin, D., Ed.; Academic Press: New York, 1978; Vol. *III*, Part A, pp 1−165.

(4) Vitasovic, M.; Gouterman, M.; Linschitz, H. *J. Porphyrins Pthalocyanines* **2001**, *05*, 191−197.

(5) Buchler, J. W.; Dreher, C.; Künzel, F. M. Synthesis and coordination chemistry of noble metal porphyrins. *Struct. Bonding* **1995**, *84*, 1−69.

(6) Antipas, A.; Dolphin, D.; Gouterman, M.; Johnson, E. C. Porphyrins. 38.1 Redox Potentials, Charge Transfer Transitions, and Emission of Copper, Silver, and Gold Complexes. *J. Am. Chem. Soc.* **1978**, *100*, 7705−7709.

(7) Papkovsky, D. B.; O'Riordan, T. C. Emerging Applications of Phosphorescent Metalloporphyrins. *J. Fluoresc.* **2005**, *15*, 569−584.

(8) Kwong, R. C.; Sibley, S.; Dubovoy, T.; Baldo, M.; Forrest, S. R.; Thompson, M. E. Efficient, Saturated Red Organic Light Emitting Devices Based on Phosphorescent Platinum(II) Porphyrins. *Chem. Mater.* **1999**, *11*, 3709−3713.

(9) Sommer, J. R.; Shelton, A. H.; Parthasarathy, A.; Ghiviriga, I.; Reynolds, J. R.; Schanze, K. S. Photophysical Properties of Near-Infrared Phosphorescent π-Extended Platinum Porphyrins. *Chem. Mater.* **2011**, *23*, 5296−5304.

(10) Briñas, R. P.; Troxler, T.; Hochstrasser, R. M.; Vinogradov, S. A. Phosphorescent Oxygen Sensor with Dendritic Protection and Two-Photon Absorbing Antenna. *J. Am. Chem. Soc.* **2005**, *127*, 11851−11862.

(11) Wu, F.; Yue, L.; Su, H.; Wang, K.; Yang, L.; Zhu, X. Carbon Dots @ Platinum Porphyrin Composite as Theranostic Nanoagent for Efficient Photodynamic Cancer Therapy. *Nanoscale Res. Lett.* **2018**, *13*, 357.

(12) Deng, J.; Li, H.; Yang, M.; Wu, F. Palladium porphyrin complexes for photodynamic cancer therapy: effect of porphyrin units and metal. *Photochem. Photobiol. Sci.* **2020**, *19*, 905−912.

(13) Kavandi, J.; Callis, J.; Gouterman, M.; Khalil, G.; Wright, D.; Green, E. Luminescent barometry in wind tunnels. *Rev. Sci. Instrum.* **1990**, *61*, 3340−3347.

(14) Khalil, G. E.; Costin, C.; Crafton, J.; Jones, G.; Grenoble, S.; Gouterman, M.; Callis, J. B.; Dalton, L. R. Dual-luminophor pressure-sensitive paint: I. Ratio of reference to sensor giving a small temperature dependency. *Sens. Actuators, B* **2004**, *97*, 13−21.

(15) Zelelow, B.; Khalil, G. E.; Phelan, G.; Carlson, B.; Gouterman, M.; Callis, J. B.; Dalton, L. R. Dual luminophor pressure sensitive paint: II. Lifetime based measurement of pressure and temperature. *Sens. Actuators, B* **2003**, *96*, 304−314.

(16) Gouterman, M. Oxygen Quenching of Luminescence of Pressure Sensitive Paint for Wind Tunnel Research. *J. Chem. Educ.* **1997**, *74*, 697−702.

(17) Ghosh, A. Electronic Structure of Corrole Derivatives: Insights from Molecular Structures, Spectroscopy, Electrochemistry, and Quantum Chemical Calculations. *Chem. Rev.* **2017**, *117*, 3798−3881.

(18) Teo, R. D.; Hwang, J. Y.; Termini, J.; Gross, Z.; Gray, H. B. Fighting Cancer with Corroles. *Chem. Rev.* **2017**, *117*, 2711−2729.

(19) Nardis, S.; Mandoj, F.; Stefanelli, M.; Paolesse, R. Metal complexes of corrole. *Coord. Chem. Rev.* **2019**, *388*, 360−405.

(20) Lemon, C. M.; Powers, D. C.; Brothers, P. J.; Nocera, D. G. Gold Corroles as Near-IR Phosphors for Oxygen Sensing. *Inorg. Chem.* **2017**, *56*, 10991−10997.

(21) Alemayehu, A. B.; Thomas, K. E.; Einrem, R. F.; Ghosh, A. The Story of 5d Metallocorroles: From Metal−Ligand Misfits to New Building Blocks for Cancer Phototherapeutics. *Acc. Chem. Res.* **2021**, *54*, 3095−3107.

(22) Einrem, R. F.; Gagnon, K. J.; Alemayehu, A. B.; Ghosh, A. Metal-Ligand Misfits: Facile Access to Rhenium-Oxo Corroles by Oxidative Metalation. *Chem. − Eur. J.* **2016**, *22*, 517−520.

(23) Borisov, S. M.; Einrem, R. F.; Alemayehu, A. B.; Ghosh, A. Ambient-temperature near-IR phosphorescence and potential applications of rhenium-oxo corroles. *Photochem. Photobiol. Sci.* **2019**, *18*, 1166−1170.

(24) Einrem, R. F.; Alemayehu, A. B.; Borisov, S. M.; Ghosh, A.; Gederaas, O. A. Amphiphilic Rhenium-Oxo Corroles as a New Class of Sensitizers for Photodynamic Therapy. *ACS Omega* **2020**, *5*, 10596−10601.

(25) Alemayehu, A. B.; Gagnon, K. J.; Terner, J.; Ghosh, A. Oxidative Metalation as a Route to Size-Mismatched Macrocyclic Complexes: Osmium Corroles. *Angew. Chem., Int. Ed.* **2014**, *53*, 14411−14414.

(26) Borisov, S. M.; Alemayehu, A.; Ghosh, A. Osmium-Nitrido Corroles as NIR Indicators for Oxygen Sensors and Triplet Sensitizers for Organic Upconversion and Singlet Oxygen Generation. *J. Mater. Chem. C* **2016**, *4*, 5822−5828.

(27) Palmer, J. H.; Durrell, A. C.; Gross, Z.; Winkler, J. R.; Gray, H. B. Near-IR Phosphorescence of Iridium(III) Corroles at Ambient Temperature. *J. Am. Chem. Soc.* **2010**, *132*, 9230−9231.

(28) Sinha, W.; Ravotto, L.; Ceroni, P.; Kar, S. NIR-Emissive Iridium(III) Corrole Complexes as Efficient Singlet Oxygen Sensitizers. *Dalton Trans.* **2015**, *44*, 17767−17773.

(29) Thomassen, I. K.; McCormick-McPherson, L. J.; Borisov, S. M.; Ghosh, A. Iridium Corroles Exhibit Weak Near-Infrared Phosphorescence but Efficiently Sensitize Singlet Oxygen Formation. *Sci. Rep.* **2020**, *10*, 7551.

(30) Alemayehu, A. B.; Vazquez-Lima, H.; Beavers, C. M.; Gagnon, K. J.; Bendix, J.; Ghosh, A. Platinum Corroles. *Chem. Commun.* **2014**, *50*, 11093−11096.
(31) Alemayehu, A. B.; McCormick, L. J.; Gagnon, K. J.; Borisov, S. M.; Ghosh, A. Stable Platinum(IV) Corroles: Synthesis, Molecular Structure, and Room-Temperature Near-IR Phosphorescence. *ACS Omega* **2018**, *3*, 9360−9368.
(32) Alemayehu, A. B.; Ghosh, A. Gold Corroles. *J. Porphyrins Phthalocyanines* **2011**, *15*, 106−110.
(33) Rabinovitch, E.; Goldberg, I.; Gross, Z. Gold(I) and Gold(III) Corroles. *Chem. − Eur. J.* **2011**, *17*, 12294−12301.
(34) Thomas, K. E.; Alemayehu, A. B.; Conradie, J.; Beavers, C.; Ghosh, A. Synthesis and Molecular Structure of Gold Triarylcorroles. *Inorg. Chem.* **2011**, *50*, 12844−12851.
(35) Alemayehu, A. B.; Jae Day, N. U.; Mani, T.; Rudine, A. B.; Thomas, K. E.; Gederaas, O. A.; Vinogradov, S. A.; Wamser, C. C.; Ghosh, A. Gold Tris(carboxyphenyl)corroles as Multifunctional Materials: Room Temperature Near-IR Phosphorescence and Applications to Photodynamic Therapy and Dye-Sensitized Solar Cells. *ACS Appl. Mater. Interfaces* **2016**, *8*, 18935−18942.
(36) For a comprehensive introduction to TDDFT, see: Ullrich, C. A. *Time-Dependent Density-Functional Theory: Concepts and Applications*; Oxford University Press: Oxford, U. K., 2011.
(37) Alemayehu, A. B.; Conradie, J.; Ghosh, A. A First TDDFT Study of Metallocorrole Electronic Spectra: Copper *meso*-Triarylcorroles Exhibit *Hyper* Spectra. *Eur. J. Inorg. Chem.* **2011**, *12*, 1857−1864.
(38) Conradie, J.; Wamser, C. C.; Ghosh, A. Understanding Hyperporphyrin Spectra: TDDFT Calculations on Diprotonated Tetrakis(*p*-aminophenyl)porphyrin. *J. Phys. Chem. A* **2021**, previous article in this issue: DOI: 10.1021/acs.jpca.1c06621.
(39) Dorough, G. D.; Miller, J. R.; Huennekens, F. M. Spectra of the Metallo-derivatives of *α*,*β*,*γ*,*δ*-Tetraphenylporphine. *J. Am. Chem. Soc.* **1951**, *73*, 4315−4320.
(40) Edwards, L.; Dolphin, D. H.; Gouterman, M.; Adler, A. D. Porphyrins XVII. Vapor absorption spectra and redox reactions: Tetraphenylporphins and porphin. *J. Mol. Spectrosc.* **1971**, *38*, 16−32.
(41) Thomas, D. W.; Martell, A. E. Visible and ultraviolet absorption spectra of metal chelates of *para*-substituted tetraphenylporphines. *Arch. Biochem. Biophys.* **1958**, *76*, 286−294.
(42) Mink, L. M.; Neitzel, M. L.; Bellomy, L. M.; Falvo, R. E.; Boggess, R. K.; Trainum, B. T.; Yeaman, P. Platinum(II) and platinum(IV) porphyrin complexes: synthesis, characterization, and electrochemistry. *Polyhedron* **1997**, *16*, 2809−2817.
(43) The calculated data on Al^{III}[TPC]$(NH_3)_2$ have been compared to experimental data on Al^{III}[TPFPC]$(py)_2$ Mahammed, A.; Gross, Z. Aluminum Corrolin, A Novel Chlorophyll Analogue. *J. Inorg. Biochem.* **2002**, *88*, 305−309.
(44) Velde, G. T.; Bickelhaupt, F. M.; Baerends, E. J.; Guerra, C. F.; van Gisbergen, S. J. A.; Snijders, J. G.; Ziegler, T. Chemistry with ADF. *J. Comput. Chem.* **2001**, *22*, 931−967.
(45) Handy, N. C.; Cohen, A. J. Left-right correlation energy. *Mol. Phys.* **2001**, *99*, 403−412.
(46) Lee, C.; Yang, W.; Parr, R. G. Development of the Colle-Salvetti correlation-energy formula into a functional of the electron density. *Phys. Rev. B* **1988**, *37*, 785−789.
(47) Grimme, S.; Anthony, J.; Ehrlich, S.; Krieg, H. A Consistent and Accurate *Ab Initio* Parametrization of Density Functional Dispersion Correction (DFT-D) for the 94 Elements H-Pu. *J. Chem. Phys.* **2010**, *132*, 154104.
(48) Seth, M.; Ziegler, T. Range-Separated Exchange Functionals with Slater-Type Functions. *J. Chem. Theory Comput.* **2012**, *8*, 901−907.
(49) Note that CAMY-B3LYP is the Yukawa form of CAM-B3LYP[51] with $a = 0.19$ and $b = 0.46$ (and $g = 0.34$) but with the Yukawa potential as the switching function, as opposed to the Coulomb potential attenuated by the complementary error function.
(50) Yanai, T.; Tew, D. P.; Handy, N. C. A new hybrid exchange-correlation functional using the Coulomb-attenuating method (CAM-B3LYP). *Chem. Phys. Lett.* **2004**, *393*, 51−57.
(51) Becke, A. D. Density-functional exchange-energy approximation with correct asymptotic behaviour. *Phys. Rev. A* **1988**, *38*, 3098−3100.
(52) Miehlich, B.; Savin, A.; Stoll, H.; Preuss, H. Results Obtained with the Correlation Energy Density Functionals of Becke and Lee, Yang and Parr. *Chem. Phys. Lett.* **1989**, *157*, 200−206.
(53) Klamt, A.; Schürmann, G. COSMO: A New Approach to Dielectric Screening in Solvents with Explicit Expressions for the Screening Energy and Its Gradient. *J. Chem. Soc., Perkin Trans. 2* **1993**, 799−805.
(54) Matson, B.; Thomas, K. E.; Alemayehu, A. B.; Ghosh, A.; Sarangi, R. X-ray absorption spectroscopy of exemplary platinum porphyrin and corrole derivatives: metal- versus ligand-centered oxidation. *RSC Adv.* **2021**, *11*, 32269-32274. Correction. *RSC Adv.* **2021**, *11*, 33300−33300.
(55) Thomassen, I. K.; Ghosh, A. Protonation-Induced Hyperporphyrin Spectra of meso-Aminophenylcorroles. *ACS Omega* **2020**, *5*, 9023−9030.

https://doi.org/10.1021/acs.jpca.1c08425
J. Phys. Chem. A 2021, 125, 9962−9968